Error study of a hybrid testing system of structures through a state-space model

F. J. Molina, A. Bosi, P. Pegon, G. Magonette & A. Pinto
European Commission, JRC, IPSC,European Laboratory for Structural Assessment, Italy.

SUMMARY:
Experimental methods such as hybrid or pseudo-dynamic tests are always subjected to experimental errors which effect on the obtained response is important to assess. An analytical linear model formulated on state-space equations has been developed for a multi DoF hybrid testing system including the components of the control and the specimen. For an example of a single DoF steel frame, the parameters of the model have been calibrated through comparison with experimental data of the control system. The model has been used to predict in pseudo-dynamic tests on such specimen the control errors and their consequences in terms of eigenfrequency and damping distortion in the test response. These predictions match with the observed experimental data and allow understanding, for example, the effects on the response of performing the test at different testing speeds or for different parameter configurations of the control algorithm.

Keywords: Hybrid test, pseudo-dynamic test, linear model, control errors, testing errors.

1. INTRODUCTION

Experimental methods such as hybrid or pseudo-dynamic (PsD) tests are used for validation of the response of structures to earthquakes and other dynamic actions. However, these experiments are always subjected to experimental errors, such as control errors, which effect on the obtained response is important to assess so that the reliability of the results can be guaranteed (Shing and Mahin, 1987, Thewalt and Roman, 1994, Molina et al., 2002, Mosqueda et al., 2007).
A linear analytical multi-DoF model of a complete PsD testing system was developed and calibrated by means of comparison with experimental results as reported by Molina et al. (2010). The model considered for the physical part a linear structure specimen, the compressibility of the oil in the hydraulic actuators, its leakage between the cylinder chambers and the internal friction of the pistons. The model described in this article (Molina et al., 2012b) constitutes an improvement of that one. With respect to the components of the hydraulic devices, it introduces a second-order servo-valve model, which allows applying the model to higher frequencies that can be relevant for fast hybrid tests. The control algorithm is based on a PID formula on the control error, but includes also additional parameters on error second derivative and feed-forward velocity and acceleration, as well as the measured force and the pressure difference between the cylinder chambers. Finally, with respect to the testing method, it considers a general category of hybrid tests that may include also numerical substructuring.
For an example of a SDoF steel frame, the physical parameters of the model have been calibrated through comparison with experimental FRFs of the control system. With respect to its previous version that considered purely proportional servo-valves, this current model is able to reproduce the experimental FRFs with accuracy in a wider range of frequencies that arrives now up to 8 Hz. In order to have the best match with the experimental curves, the parameters of the linear model need to be adjusted to the working amplitude of the test. However this is not a big barrier for the purpose of describing the general behaviour of the expected errors within that range of frequency during a hybrid test. The analytical model has been used to study the behaviour of the testing method in the presence

of control errors and how this is modified by the control and the testing parameters. The analytical results have been successfully compared (Molina et al., 2011a, 2012b) with monitoring techniques applied to the experiments (Molina et al., 2011b) in order to validate also the reliability of those monitoring techniques.
This article describes the principles of the formulation of the model and presents the results of a parametric study performed with it for the SDoF example. The effect on the testing errors in terms of response eigenfrequency and damping ratio is shown as a function of the control parameters and the testing speed.

2. MODEL OF THE CONTROL SYSTEM

This section develops an analytical linear model for the control system of a M-DoF specimen using M actuators. Fig. 1 shows a schematic representation of the model (Molina et al., 2012b). The equations regarding the servo-valve, the actuator, the specimen and the controller are formulated as follows.

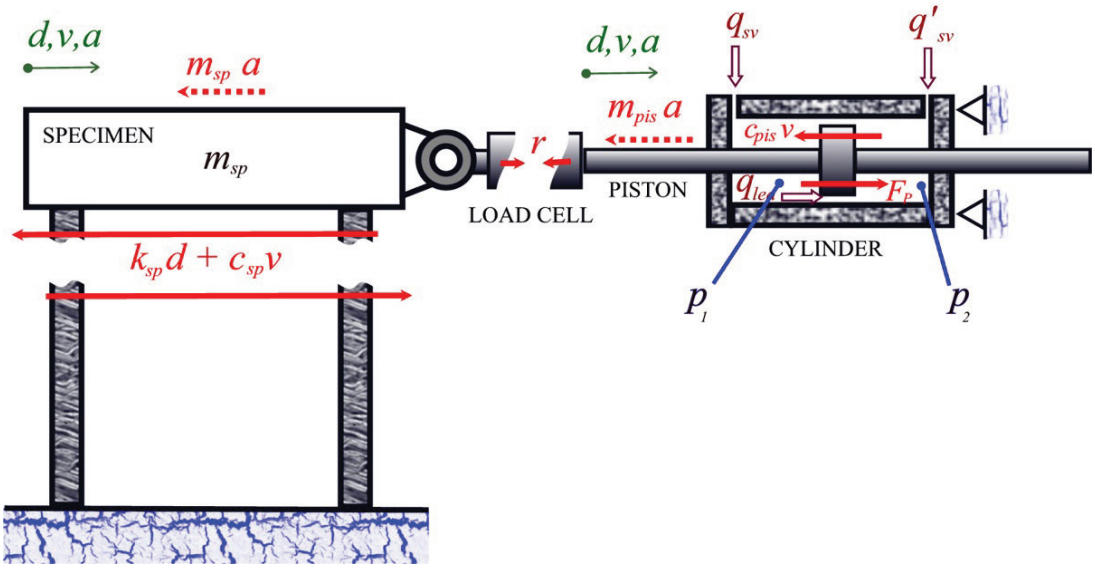

Figure 1. Model of the control system.

Linear geometrical and static transformations between the M displacements at the DoFs of the specimen $\mathbf{d}_{sp}$ and the displacements of the M pistons $\mathbf{d}_{pis}$, as well as between the piston load cell forces $\mathbf{r}_{pis}$ and the specimen restoring forces $\mathbf{r}_{sp}$ are assumed. That is,

$$\mathbf{d}_{pis}(t) = \mathbf{T}\mathbf{d}_{sp}(t), \qquad \mathbf{r}_{sp}(t) = \mathbf{T}^T\mathbf{r}_{pis}(t) \tag{1}$$

where $\mathbf{T}$ is a constant transformation matrix and t is the time variable.
Regarding the servo-valve model, for a range of small oscillations around an equilibrium position of zero force on the piston, the two-way oil flow rate will be assumed proportional to the spool displacement

$$\mathbf{q}_{SV}(t) = \mathbf{k}_{SV}\mathbf{d}_{SV}(t) \tag{2}$$

where $\mathbf{k}_{SV}$ is the diagonal matrix of flow-gain coefficients. The displacement of the spool of the servo-valves $\mathbf{d}_{SV}$ is assumed to follow, as described in the literature (e.g., Plummer, 2008), the servo-

valve reference input signal $\mathbf{d}_{SV}^{r}$, according to a second order transfer function. In the state space, this will be expressed as

$$\dot{\mathbf{d}}_{SV}(t)=\mathbf{v}_{SV}(t);\qquad \dot{\mathbf{v}}_{SV}(t)=\boldsymbol{\omega}_{SV}^{2}\mathbf{d}_{SV}^{r}(t)-\boldsymbol{\omega}_{SV}^{2}\mathbf{d}_{SV}(t)-2\boldsymbol{\zeta}_{SV}\boldsymbol{\omega}_{SV}\mathbf{v}_{SV}(t) \tag{3}$$

where $\mathbf{v}_{SV}$ is the spool velocity and $\boldsymbol{\omega}_{SV}$ and $\boldsymbol{\zeta}_{SV}$ are, respectively, the servo-valve natural frequency and damping ratio. The servo-valve input signal is proportional to the controller command, i.e.,

$$\mathbf{d}_{SV}^{r}(t)=\mathbf{k}_{con}\,\mathbf{c}_{con}(t) \tag{4}$$

The rate of the hydraulic forces on the pistons $\mathbf{F}_{P}(t)$ will be determined through the oil column stiffnesses $\mathbf{k}_{oil}$, by the servo-valve oil fluxes and piston velocities ($\mathbf{v}_{pis}(t)=\dot{\mathbf{d}}_{pis}(t)$), as well as by the leakage between the cylinder chambers, i.e.,

$$\dot{\mathbf{F}}_{P}(t)=\mathbf{k}_{oil}\left[\mathbf{A}_{pis}^{-1}\mathbf{q}_{SV}(t)-\mathbf{v}_{pis}(t)\right]-\boldsymbol{\tau}_{lea}^{-1}\,\mathbf{F}_{P}(t) \tag{5}$$

where $\mathbf{A}_{pis}$ are the piston sections and $\boldsymbol{\tau}_{lea}$ are the time constants of leakage.
For the model of the specimen we will consider the dynamic equilibrium equations

$$\mathbf{m}_{sp}\mathbf{a}_{sp}(t)+\mathbf{c}_{sp}\mathbf{v}_{sp}(t)+\mathbf{k}_{sp}\mathbf{d}_{sp}(t)=\mathbf{r}_{sp}(t) \tag{6}$$

where $\mathbf{a}_{sp}$, $\mathbf{v}_{sp}$, $\mathbf{d}_{sp}$ and $\mathbf{r}_{sp}$ are respectively the acceleration, velocity, displacement and restoring force vectors of the specimen and $\mathbf{m}_{sp}$, $\mathbf{c}_{sp}$ and $\mathbf{k}_{sp}$, are respectively its matrices of mass, damping and stiffness. By free-body equilibrium, the load cell forces can be written as a function of the other forces acting on the pistons

$$\mathbf{r}_{pis}(t)=\mathbf{F}_{P}(t)-\mathbf{m}_{pis}\mathbf{a}_{pis}(t)-\mathbf{c}_{pis}\mathbf{v}_{pis}(t) \tag{7}$$

where $\mathbf{m}_{pis}$ and $\mathbf{c}_{pis}$ are respectively the diagonal piston matrices of mass and internal damping.
Then, by introducing (1) and (7) in (6),

$$\dot{\mathbf{v}}_{sp}(t)=\left(\mathbf{m}_{sp}+\mathbf{T}^{T}\mathbf{m}_{pis}\mathbf{T}\right)^{-1}\left[\mathbf{T}^{T}\mathbf{F}_{P}(t)-\left(\mathbf{c}_{sp}+\mathbf{T}^{T}\mathbf{c}_{pis}\mathbf{T}\right)\mathbf{v}_{sp}(t)-\mathbf{k}_{sp}\mathbf{d}_{sp}(t)\right] \tag{8}$$

The digital controller is approximated by an analogue control law

$$\begin{aligned}\mathbf{c}_{con}(t)=\mathbf{k}_{P}\Big[&\boldsymbol{\varepsilon}(t)+\mathbf{k}_{I}{}^{-1}\boldsymbol{\varepsilon}_{I}(t)+\mathbf{k}_{D}\dot{\boldsymbol{\varepsilon}}(t)+\mathbf{k}_{A}\ddot{\boldsymbol{\varepsilon}}(t)\\&+\mathbf{k}_{VFF}\mathbf{v}_{pis}^{r}(t)+\mathbf{k}_{AFF}\mathbf{a}_{pis}^{r}(t)+\mathbf{k}_{r}\mathbf{r}_{pis}(t)+\mathbf{k}_{\Delta P}\Delta\mathbf{P}(t)\Big]\end{aligned} \tag{9}$$

within this model, where, respectively, $\mathbf{k}_{P}$, $\mathbf{k}_{I}$, $\mathbf{k}_{D}$ and $\mathbf{k}_{A}$ are the matrices containing the proportional, integral, derivative and second-derivative gains on the control error, $\mathbf{k}_{VFF}$ and $\mathbf{k}_{AFF}$ are the feed-forward gains on the velocity and acceleration of the reference signal and, finally, $\mathbf{k}_{r}$ and

$\mathbf{k}_{\Delta P}$ contain the load-cell and differential-pressure gains. The error signal vector is computed as the difference between the reference (target) displacement $\mathbf{d}^r_{pis}$ and the measured displacement $\mathbf{d}_{pis}$

$$\boldsymbol{\varepsilon}(t) = \mathbf{d}^r_{pis}(t) - \mathbf{d}_{pis}(t) = \mathbf{T}\mathbf{d}^r_{sp}(t) - \mathbf{T}\mathbf{d}_{sp}(t) \tag{10}$$

The integrated error verifies by definition

$$\dot{\boldsymbol{\varepsilon}}_I(t) = \boldsymbol{\varepsilon}(t) = \mathbf{T}\mathbf{d}^r_{sp}(t) - \mathbf{T}\mathbf{d}_{sp}(t) \tag{11}$$

Finally, we will express the model of the control system by the state equations

$$\dot{\mathbf{x}}_{cs}(t) = \mathbf{A}_{cs}\mathbf{x}_{cs}(t) + \mathbf{B}_{cs}\mathbf{u}_{cs}(t) \tag{12}$$

where, by choice,

$$\begin{aligned} \mathbf{x}_{cs}(t) &= \left[\mathbf{d}_{sp}(t) \quad \mathbf{v}_{sp}(t) \quad \mathbf{F}_P(t) \quad \boldsymbol{\varepsilon}_I(t) \quad \mathbf{d}_{SV}(t) \quad \mathbf{v}_{SV}(t)\right]^T \\ \mathbf{u}_{cs}(t) &= \left[\mathbf{d}^r_{sp}(t) \quad \mathbf{v}^r_{sp}(t) \quad \mathbf{a}^r_{sp}(t)\right]^T \end{aligned} \tag{13}$$

are the state and input vectors respectively. The derivation from the previous equations of the formulas for the coefficients of the system matrices is given by Molina et al. (2012b).

3. MODEL OF THE HYBRID TESTING SET-UP

The hybrid test will consist of the numerical integration of an equation of motion of the type

$$\mathbf{m}^{an}_{hyb}\frac{d^2}{dT^2}\mathbf{d}_{hyb}(T) + \mathbf{c}^{an}_{hyb}\frac{d}{dT}\mathbf{d}_{hyb}(T) + \mathbf{k}^{an}_{hyb}\mathbf{d}_{hyb}(T) + \mathbf{r}^{meas}_{hyb}(T) = \mathbf{f}^{INP}_{hyb}(T) \tag{14}$$

where T is the prototype time variable. This prototype time coincides with the laboratory time only in the case of a real-time test. Otherwise, for a scaled-time PsD test, the laboratory time will be several times larger than the prototype time, that is, $t = \lambda T$, being λ the time scale factor. We will assume within this model that the errors introduced by the numerical integration of this equation are negligible. This is not a general case, but could be applied for most of the integration methods when it is affordable to use them with a sufficiently small time increment.
Equation (14) will be rewritten for the laboratory time as

$$\mathbf{m}^{an}_{hyb}\lambda^2\ddot{\mathbf{d}}_{hyb}(t) + \mathbf{c}^{an}_{hyb}\lambda\dot{\mathbf{d}}_{hyb}(t) + \mathbf{k}^{an}_{hyb}\mathbf{d}_{hyb}(t) + \mathbf{r}^{meas}_{hyb}(t) = \mathbf{f}^{INP}_{hyb}(t) \tag{15}$$

where $\mathbf{d}_{hyb}$ is the whole vector of displacements (analytical and experimental DoFs) in the hybrid system, from which the reference displacements for the control system will be derived as

$$\mathbf{d}^r_{sp}(t) = \mathbf{L}^{hyb}_{sp}\mathbf{d}_{hyb}(t) \tag{16}$$

being $\mathbf{L}^{hyb}_{sp}$ the compatibility transformation matrix. Also in (24), $\mathbf{r}^{meas}_{hyb}$ are the measured forces,

conjugate of $\mathbf{d}_{hyb}$, that is,

$$\mathbf{r}_{hyb}^{meas}(t) = \mathbf{L}_{hyb}^{sp}\mathbf{r}_{sp}(t) = \mathbf{L}_{hyb}^{sp}\left[\mathbf{m}_{sp}\mathbf{a}_{sp}(t) + \mathbf{c}_{sp}\mathbf{v}_{sp}(t) + \mathbf{k}_{sp}\mathbf{d}_{sp}(t)\right] \tag{17}$$

where $\mathbf{r}_{sp}(t)$ are the restoring forces in the specimen as measured from the load cells of the actuators according to equation (1), $\mathbf{L}_{hyb}^{sp}$ is the required equilibrium transformation matrix and (11) has been used. The mass, damping and stiffness matrices that appear in equation (15) are the analytical representation of the properties of the hybrid system that are not physically present in the specimen. For example, in the case of a linear specimen, in order to represent a linear goal hybrid system defined by the equation

$$\mathbf{m}_{hyb}^{goal}\lambda^2\ddot{\mathbf{d}}_{hyb}(t) + \mathbf{c}_{hyb}^{goal}\lambda\dot{\mathbf{d}}_{hyb}(t) + \mathbf{k}_{hyb}^{goal}\mathbf{d}_{hyb}(t) = \mathbf{f}_{hyb}^{INP}(t) \tag{18}$$

those matrices should be defined as:

$$\begin{aligned}
\mathbf{m}_{hyb}^{an} &= \mathbf{m}_{hyb}^{goal} - (1/\lambda^2)\mathbf{L}_{hyb}^{sp}\mathbf{m}_{sp}\mathbf{L}_{sp}^{hyb} \\
\mathbf{c}_{hyb}^{an} &= \mathbf{c}_{hyb}^{goal} - (1/\lambda)\mathbf{L}_{hyb}^{sp}\mathbf{c}_{sp}\mathbf{L}_{sp}^{hyb} \\
\mathbf{k}_{hyb}^{an} &= \mathbf{k}_{hyb}^{goal} - \mathbf{L}_{hyb}^{sp}\mathbf{k}_{sp}\mathbf{L}_{sp}^{hyb}
\end{aligned} \tag{19}$$

Note that in case of a hybrid test without substructuring for a specimen having only hysteretic damping, the analytical stiffness and damping matrices should be null, whereas the analytical mass matrix should still be computed according to equation (19).
Finally, the independent term in equation (15) for the case of seismic excitation would be computed as

$$\mathbf{f}_{hyb}^{INP}(t) = -\mathbf{m}_{hyb}^{goal}\mathbf{J}\mathbf{a}_g(t) \tag{20}$$

Where $\mathbf{a}_g$ is the vector of ground accelerograms and $\mathbf{J}$ is the geometric influence matrix for those accelerograms on the DoFs of the hybrid system.

Now, as a preparation for the state equations, by calling $\mathbf{v}_{hyb}(t) = \dot{\mathbf{d}}_{hyb}(t)$, equation (15) can be rewritten as

$$\begin{aligned}
\dot{\mathbf{v}}_{hyb}(t) = \left(\mathbf{m}_{hyb}^{an}\lambda^2\right)^{-1}\Big[&\mathbf{f}_{hyb}^{INP}(t) - \mathbf{c}_{hyb}^{an}\lambda\mathbf{v}_{hyb}(t) - \mathbf{k}_{hyb}^{an}\mathbf{d}_{hyb}(t) \\
&-\mathbf{L}_{hyb}^{sp}\left(\mathbf{m}_{sp}\dot{\mathbf{v}}_{sp}(t) + \mathbf{c}_{sp}\mathbf{v}_{sp}(t) + \mathbf{k}_{sp}\mathbf{d}_{sp}(t)\right)\Big]
\end{aligned} \tag{22}$$

Where (17) has been used.
In conclusion, the state equation for the hybrid test model is written as

$$\dot{\mathbf{x}}(t) = \mathbf{A}\mathbf{x}(t) + \mathbf{B}\mathbf{u}(t) \tag{22}$$

where, by choice,

$$\mathbf{x}(t) = \left[\mathbf{d}_{hyb}(t) \quad \mathbf{v}_{hyb}(t) \quad \mathbf{x}_{cs}(t)\right]^T \quad ; \quad \mathbf{u}(t) = \left[\mathbf{f}_{hyb}^{INP}(t)\right] \tag{23}$$

are the state and input vectors respectively and $\mathbf{x}_{cs}$ are the state variables of the control system as defined by equation (13). The derivation from the previous equations of the formulas for the coefficients of the system matrices is given by Molina et al. (2012b).

4. PARAMETRIC STUDY OF TESTING ERRORS EFFECTS IN A SDOF EXAMPLE

The developed analytical model was calibrated for a 1-DoF specimen, controlled by two 20 ton actuators, tested by using the ELSA testing system. The one-storey 4-column steel frame NEFOREEE with cube shape of 3x3x3 m and a top slab mass of 8 tons was used as structure . This almost linear specimen had a natural frequency of 2.6 Hz and an equivalent damping ratio of 0.5%. The whole testing set-up as well as the sine chirp test that was performed for different configurations of the control in order to obtain the experimental FRFs of the control system were reported in previous works (Molina et al., 2010). Some of the parameters of the analytical model of the control system (12) were estimated before the comparison with the experimental results while some other parameters (such as $\mathbf{k}_{oil}, \boldsymbol{\tau}_{lea}, \mathbf{c}_{pis}, \boldsymbol{\omega}_{SV}, \boldsymbol{\zeta}_{SV}$) were manually optimised by visual matching of the analytical and experimental FRFs. In the model with a proportional servo-valve (Molina et al., 2010) for the closed and the open-loop graphs, the obtained comparison of experimental and analytical curves was acceptable for frequencies up to more or less 5 Hz, regarding amplitude, and up to 1.5 Hz, regarding the phase. With the current model that introduces a second-order representation for the servo-valve, the matching is acceptable for frequencies up to 8 Hz, regarding both amplitude and phase (Molina et al., 2012b).

Once the calibrated parameters are got, the analytical model of the hybrid test can be used to predict the response frequency ω_{hyb} and damping ratio ζ_{hyb} of the response as they are obtained from the first pole (eigenvalue of $\mathbf{A}$) in the testing system (22). The difference between those response parameters and the ideal ones associated to the goal system (18) constitutes the error introduced in the test by the control errors. By using the spatial model identification method (Molina et al., 2011ab, 2012a) the frequency and damping errors can be estimated from the test results. A successful comparison of the estimated errors from a series of PsD experiments and the analytical model predictions has been done for the SDoF example, initially with the proportional servo-valve model (Molina et al., 2011a) and more recently with the second order servo-valve model (Molina et al., 2012b). It has been observed that, at the scaled frequencies of the PsD test, the non-proportional behaviour of the servo-valve has no effect. In fact, the fastest test was conducted with $\lambda = 20$, that corresponds to an ideal response frequency of 2.6/20=0.13 Hz, which is in the range of accuracy (0-1.5 Hz) for this set-up with the simpler model based on a perfect servo-valve.

For the current parametric study, apart from the testing speed λ, having in mind the control law (9), the parameters that will be used are M_G, $\mathbf{k}_P$, $\mathbf{k}_I$, $\mathbf{k}_D$, $\mathbf{k}_A$, $\mathbf{k}_{VFF}$, $\mathbf{k}_{AFF}$, $\mathbf{k}_{\Delta P}$, $\mathbf{k}_r$, where M_G is the gain margin, defined as the maximum scalar by which a given proportional gain $\mathbf{k}_P$ can be multiplied without losing the stability, i.e., all the poles of the control system (12) must keep their real part negative. In this study, we will impose as a constrain a constant gain margin of 10, which is a safe recommendable value according to our experience. Thus, for the given testing set-up, once the value of all the control parameters is specified, except from $\mathbf{k}_P$, the value of this gain will be determined from that constrain.

For each parameter, except the time scale, a figure will be produced that considers the variation of this parameter in the abscissa, keeping the remaining parameters fixed to the default values:

$$I = 1000\,\mathbf{k}_I = 500, \quad D = 1000\,\mathbf{k}_D = 0, \quad \mathbf{k}_A = \mathbf{k}_{VFF} = \mathbf{k}_{AFF} = \mathbf{k}_{\Delta P} = \mathbf{k}_r = 0 \tag{24}$$

Then, each figure will contain three graphs. The upper graph will show the evolution of the response frequency relative error in the hybrid test. The middle graph will illustrate the response damping ratio error. And the lower graph will show the evolution of the proportional gain parameter $P = \mathbf{k}_P / 1000$

as required to satisfy the imposed gain margin of 10. In all the graphs, the solid line will refer to the testing speed $\lambda = 20$, and the dashed line will refer to $\lambda = 40$.

The effect of the variation of the integral gain parameter $I = 1000\,\mathbf{k}_I$ is shown in the left side of Fig. 2. The two upper graphs show how the frequency and damping errors can be diminished by reducing the value of this parameter, while according to the lower graph, the proportional gain needs to be reduced in order to keep constant gain margin of stability. However, there is a lower limit for the I parameter as is made more evident in the zoom of the right side of Fig. 2. The errors are minimum for I between 12 and 14 (depending on the type of error and on the testing speed). Going under this inferior limit, they grow very fast and P approaches zero.

Left side of Fig. 3 shows the effect of the variation of the derivative gain parameter $D = 1000\,\mathbf{k}_D$. The two upper graphs show how the frequency and damping errors grow either by increasing or decreasing the value of this parameter, while the proportional gain needs to be reduced in both cases according to the lower graph, in order to keep constant gain margin of stability. Starting from the defined default values of the parameters, there is no advantage in introducing any variation of this parameter for this example. Right side of Fig. 3 shows the effect of the variation of the second derivative gain parameter $\mathbf{k}_A$. From the default configuration, by introducing positive values of this parameter the proportional gain can be largely increased, keeping the same stability margin and largely reducing at the same time the frequency and damping errors of the test. This is true up to an upper limit around $\mathbf{k}_A = 1.6 \bullet 10^{-3}$, after which all these tendencies are inverted.

Left side of Fig. 4 shows the effect of the variation of the feed-forward velocity gain parameter $\mathbf{k}_{VFF}$. This parameter does not affect the feedback of the closed loop and consequently has no influence in the stability (the required proportional gain is not modified by it). It can make reduce the frequency and damping errors of the test, even down to zero, but the required value of it is not the same for the zero of the frequency error as for the zero of the damping error. This also depends on the testing speed. Right side of Fig. 4 shows the effect of the variation of the feed-forward acceleration gain parameter $\mathbf{k}_{AFF}$. This parameter, as the previous one, has no effect on the required proportional gain for stability. It can make reduce the frequency or damping errors of the test, but not at the same time. This parameter and the previous one, when combined, can be interpreted as a 2-parameter filter that modifies the reference signal, without affecting the feedback, and that can be used to compensate on a particular band of frequency for the deficiencies of the rest of the control system. Probably, the right way to use these two parameters would be to optimise their values in combination so that, at least for one testing speed, both errors (frequency and damping) are set as close as possible to zero.

Left side of Fig. 5 shows the effect of the variation of the load-cell gain parameter $\mathbf{k}_r$. For this example, negative values of this parameter behave in a similar way as the positive values of the $\mathbf{k}_A$ parameter. It allows to increase drastically the proportional gain, for a constant gain margin, and this simultaneously reduces all the errors. The lower limit for these positive effects is around $\mathbf{k}_r = -2.2 \bullet 10^{-8}$. Finally, right side of Fig. 5 shows the effect of the variation of the pressure difference gain parameter $\mathbf{k}_{\Delta P}$. As for the previous parameter, negative values make increase the proportional gain and reduce all the errors. The lower limit for these positive effects is around $\mathbf{k}_{\Delta P} = -2.7 \bullet 10^{-10}$. However, as a difference with respect to the behaviour of the $\mathbf{k}_A$ and $\mathbf{k}_r$ parameters, the use of a value of it that is close to the one that minimizes the errors is dangerous in this case because of an apparently explosive behaviour of the errors and the required proportional gain in the vicinity as observed in the graphs.

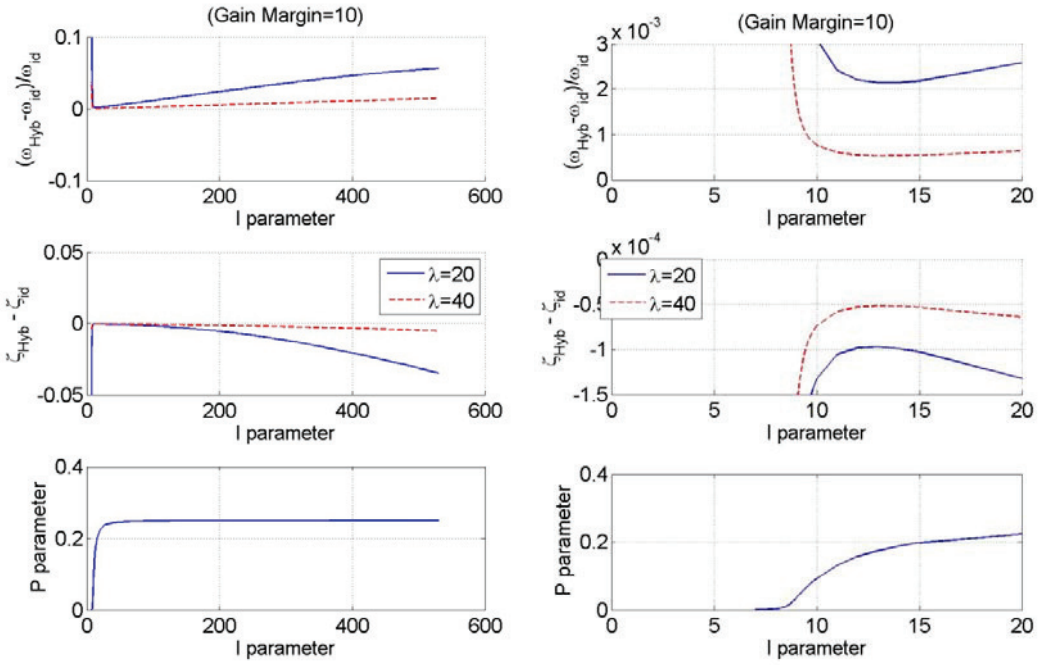

Figure 2. Variation of error integral gain parameter (left) and zoom of the same graphs (right).

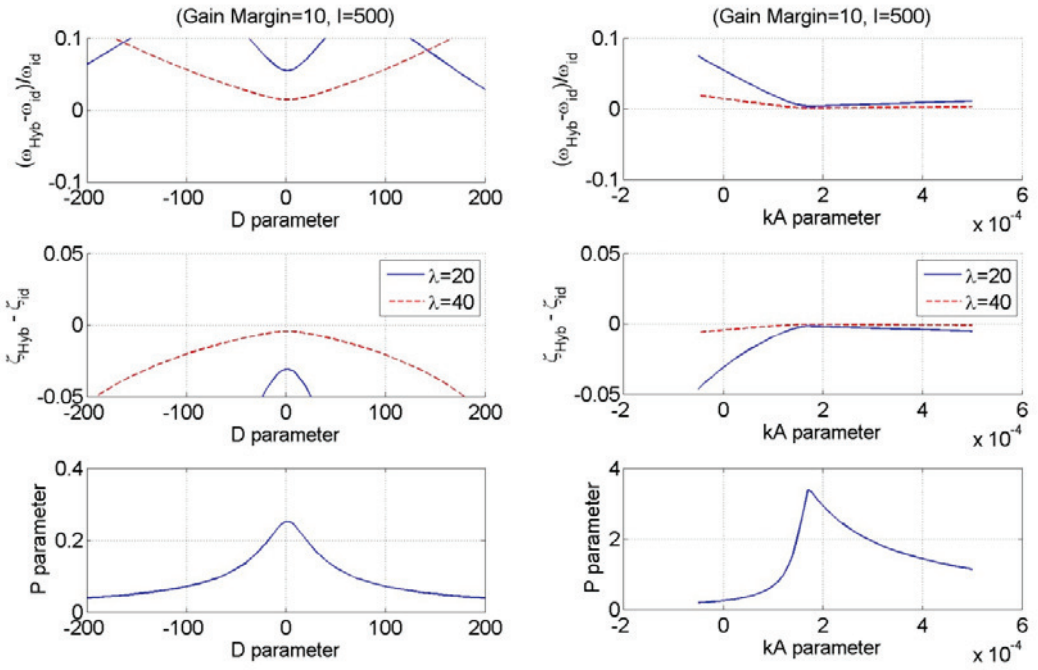

Figure 3. Variation of error derivative gain (left) and error acceleration gain (right).

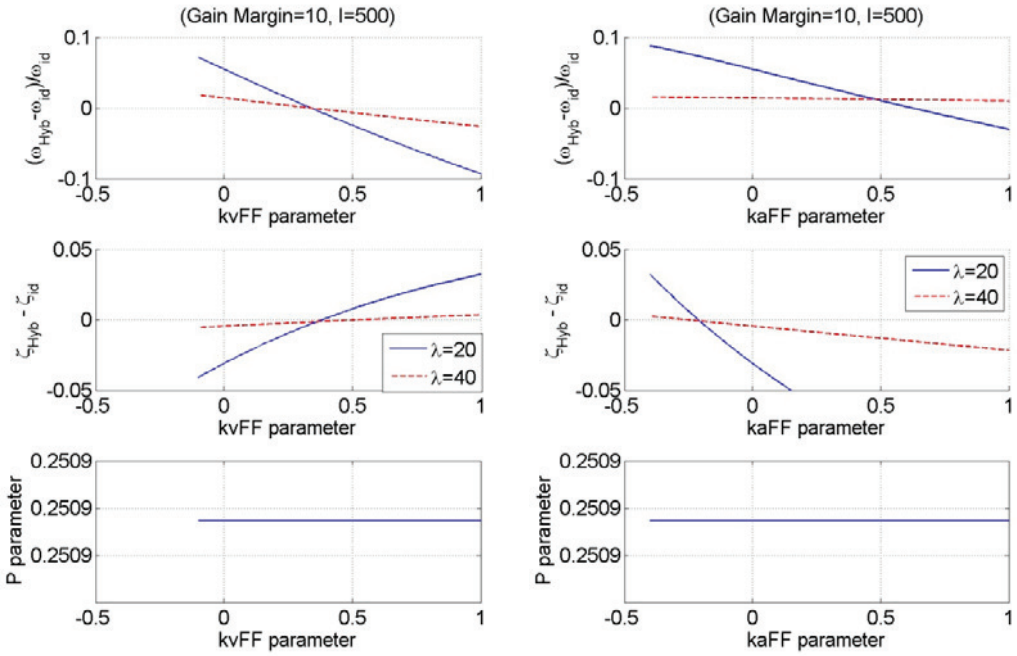

Figure 4. Variation of velocity feed-forward gain (left) and acceleration feed-forward gain (right).

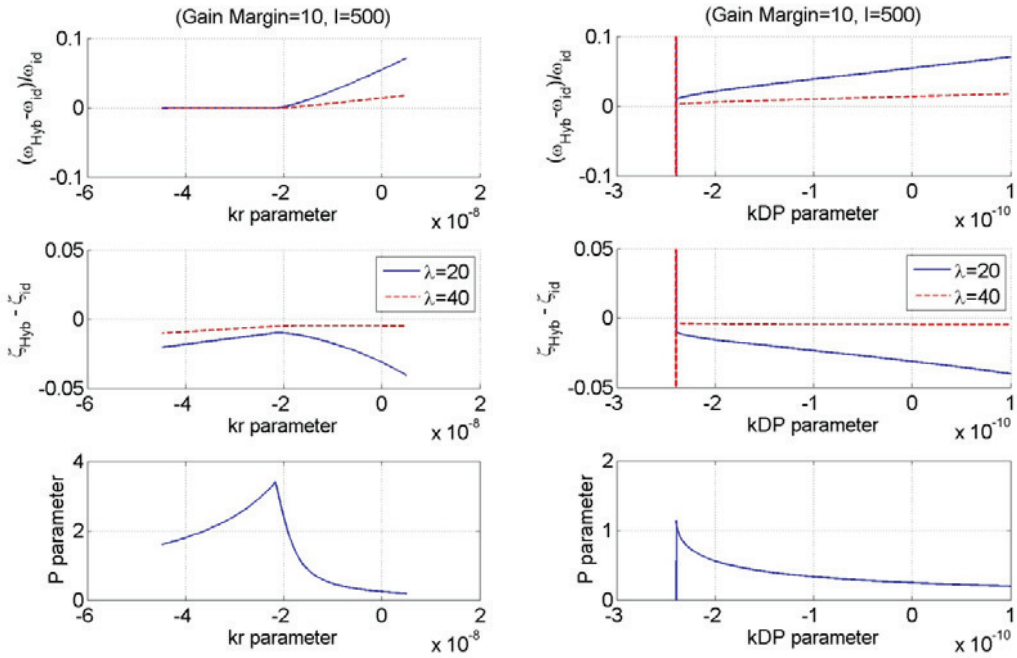

Figure 5. Variation of load-cell gain (left) and pressure-difference gain (right).

5. CONCLUSIONS

A linear model of a system for hybrid testing has been developed that includes the most important aspects of the control system regarding the quality of the tests. The formulation is able to deal with

several DoFs in the specimen controlled by several actuators. The model of the hydraulic actuators is done with symmetric pistons and considers the compressibility of the oil, the leakage between both chambers and the friction of the piston in the cylinder. A second order representation of the servo-valve has been introduced so that the response at medium frequencies can also be covered as this may be important for the stability of the control system and for characterising its performance in dynamic tests. The model includes PID control loop with additional feed-forward on reference velocity and acceleration and differential pressure and load cell terms.

After the calibration through experimental data of the parameters of the developed analytical model for a SDoF example, a parametric study of the effect of the control parameters on the testing errors has been conducted. This study allows to see how in order to reduce the testing errors for this example, a first group of the defined control parameters may help and be optimised independently of the testing speed (and presumably the natural frequency of the specimen), while a second group may also help, but their optimum value depends on the testing speed and the kind of error that should be minimised. To the first group belong controller gains applied to the integral of the control error or its second derivative, or applied to the load cell force or the pressure difference between the actuator chambers. To the second group belong the defined feed-forward gains applied to the velocity and the acceleration of the controller reference signal. The developed model is also expected to be used for the study of improved control algorithms or of alternative hybrid testing techniques. With the extended frequency bandwidth of application now attained after the introduction of the second-order servo-valve model, it could also be used for modelling shaking tables.

AKCNOWLEDGEMENT

The work presented in this paper was partially funded by the European Commission through the SAFECONSTRUCT institutional action n. 32003 of the IPSC of the EC-JRC as well as through the European Community's Seventh Framework Programme [FP7/2007-2013] for access to the ELSA of the EC-JRC under the SERIES grant agreement n. 227887 and the EFAST project (n. 212109). The authors acknowledge also all the collaboration from the colleagues in ELSA.

REFERENCES

Molina, F. J., Magonette, G. and Pegon, P. (2002). Assessment of systematic experimental errors in pseudodynamic tests. Proc. of the 12th European Conference on Earthquake Engineering, Elsevier Science, Paper 525.

Molina, F. J.. Magonette, G. and Viaccoz, B., (2010). Linear Model of a Pseudo-Dynamic Testing System, JRC Scientific and Technical Reports, EUR 24313 EN. Luxembourg: Publications Office of the European Union. JRC 57549.

Molina, F. J., Magonette, G., Pegon, P. and Zapico, B. (2011a): Monitoring Damping in Pseudo-Dynamic Tests, Journal of Earthquake Engineering, 15:6, 877-900.

Molina, F. J. (2011b) "Spatial and Filter Models" MATLAB functions freely available at MATLAB CENTRAL FILE EXCHANGE: http://www.mathworks.com/matlabcentral/fileexchange/32634.

Molina F.J., Marazzi, F., Viaccoz, B. and Bosi, A. (2012a). Stability and accuracy in a hybrid test example, Earthquake Engineering and Structural Dynamics. (EQE-11-0289.R1, accepted).

Molina, F. J., Magonette, G., Pegon, P. and Viaccoz, B. (2012b). Linear Model of a Hybrid Testing System, JRC Scientific and Technical Reports, EUR XXXX EN. Luxembourg: Publications Office of the European Union (in preparation).

Mosqueda, G., Stojadinovic, B. and Mahin, S. A. (2007). Real-Time Error Monitoring for Hybrid Simulation. Part I: Methodology and Experimental Verification. J. Struct. Engrg. 133 1100-1108.

Pegon, P., Molina, F. J. and Magonette, G. (2008). Continuous pseudo-dynamic testing at ELSA. Hybrid Simulation; Theory, Implementation and Applications, ed. Saouma V.E. and Sivaselvan M. V. (Taylor & Francis/Balkema) 79-88.

Plummer, A., R. (2008). A detailed dynamic model of a six-axis shaking table. Journal of Earthquake Engineering;12:4,631-62.

Shing, P. B. and Mahin, S. A. (1987). Cumulative experimental errors in pseudo-dynamic tests. Earthquake Engineering and Structural Dynamics. 15, 409-424.

Thewalt, C. and Roman, M. (1994). Performance Parameters for Pseudodynamic Tests. ASCE Journal of Struct. Eng. 120, 9.